Journal of Biomolecular Structure and Dynamics

ISSN: (Print) (Online) Journal homepage: https://www.tandfonline.com/loi/tbsd20

Potential of plant extracts in targeting SARS-CoV-2 main protease: an *in vitro* and *in silico* study

Ingrid Garcia de Araujo, José Renato Pattaro-Júnior, Cecilia Gomes Barbosa, Gisele Strieder Philippsen, Ana Rita Silva, Rafaella Sayuri Ioshino, Carolina Borsoi Moraes, Lúcio Holanda Freitas-Junior, Lillian Barros, Rosane Marina Peralta, Maria Aparecida Fernandez & Flavio Augusto Vicente Seixas

To cite this article: Ingrid Garcia de Araujo, José Renato Pattaro-Júnior, Cecilia Gomes Barbosa, Gisele Strieder Philippsen, Ana Rita Silva, Rafaella Sayuri Ioshino, Carolina Borsoi Moraes, Lúcio Holanda Freitas-Junior, Lillian Barros, Rosane Marina Peralta, Maria Aparecida Fernandez & Flavio Augusto Vicente Seixas (18 Jan 2023): Potential of plant extracts in targeting SARS-CoV-2 main protease: an *in vitro* and *in silico* study, Journal of Biomolecular Structure and Dynamics, DOI: 10.1080/07391102.2023.2166589

To link to this article: https://doi.org/10.1080/07391102.2023.2166589

JOURNAL OF BIOMOLECULAR STRUCTURE AND DYNAMICS
https://doi.org/10.1080/07391102.2023.2166589

Potential of plant extracts in targeting SARS-CoV-2 main protease: an *in vitro* and *in silico* study

Ingrid Garcia de Araujo[a], José Renato Pattaro-Júnior[a], Cecilia Gomes Barbosa[b,i,j], Gisele Strieder Philippsen[c], Ana Rita Silva[d,e,f], Rafaella Sayuri Ioshino[b], Carolina Borsoi Moraes[b], Lúcio Holanda Freitas-Junior[b], Lillian Barros[d,e], Rosane Marina Peralta[g], Maria Aparecida Fernandez[h] and Flavio Augusto Vicente Seixas[a]

[a]Department of Technology, Universidade Estadual de Maringá, Umuarama, P.R. Brazil; [b]Instituto de Ciências Biomédicas, Universidade de São Paulo, São Paulo, Brazil; [c]Universidade Federal do Paraná, Jandaia do Sul, P.R. Brazil; [d]Centro de Investigação de Montanha (CIMO), Instituto Politécnico de Bragança, Bragança, Portugal; [e]Laboratório Associado para a Sustentabilidade e Tecnologia em Regiões de Montanha, (SusTEC), Instituto Politécnico de Bragança, Bragança, Portugal; [f]Departamento de Ciencias Farmacéuticas, Facultad de Farmacia, CIETUS-IBSAL, Universidad de Salamanca, Salamanca, España; [g]Department of Biochemistry, Universidade Estadual de Maringá, Maringá, P.R. Brazil; [h]Department of Biotechnology, Genetics and Cell Biology, Universidade Estadual de Maringá, Maringá, P.R. Brazil; [i]Universidade Municipal de São Caetano do Sul (USCS), São Caetano, Brazil; [j]Bela Vista, São Paulo, Brazil

Communicated by Ramaswamy H. Sarma

ABSTRACT

The deaths caused by the covid-19 pandemic have recently decreased due to a worldwide effort in vaccination campaigns. However, even vaccinated people can develop a severe form of the disease that requires ICU admission. As a result, the search for antiviral drugs to treat these severe cases has become a necessity. In this context, natural products are an interesting alternative to synthetic medicines used in drug repositioning, as they have been consumed for a long time through traditional medicine. Many natural compounds found in plant extracts have already been shown to be effective in treating viral and bacterial diseases, making them possible hits to exploit against covid-19. The objective of this work was to evaluate the antiviral activity of different plant extracts available in the library of natural products of the Universidade Estadual de Maringá, by inhibiting the SARS-CoV-2 main protease (M^{pro}), and by preventing viral infection in a cellular model. As a result, the extract of *Cytinus hypocistis*, obtained by ultrasound, showed a M^{pro} inhibition capacity greater than 90%. In the infection model assays using Vero cells, an inhibition of 99.6% was observed, with a selectivity index of 42.7. The *in silico* molecular docking simulations using the extract compounds against M^{pro}, suggested Tellimagrandin II as the component of *C. hypocistis* extract most likely to inhibit the viral enzyme. These results demonstrate the potential of *C. hypocistis* extract as a promising source of natural compounds with antiviral activity against covid-19.

ARTICLE HISTORY
Received 29 August 2022
Accepted 1 January 2023

KEYWORDS
SARS-CoV-2; covid-19; *Cytinus hypocistis*; tannins; Tellimagrandin II

1. Introduction

The covid-19 is an infectious disease caused by the severe acute respiratory syndrome novel coronavirus (SARS-CoV-2), which rapidly became a pandemic, affecting more than 300 million people worldwide and leading to the death of more than 5 million individuals to date (Huang et al., 2020).

Coronaviruses (CoVs) are part of the *Coronaviridae* family that belongs to the order Nidovirales and comprise a group of diverse enveloped viruses with a single-stranded and positive-sense RNA genome. The viruses in this group act as etiological agents of various respiratory, enteric, hepatic, and neurological pathologies, having infective capacity in several animal species, with different degrees of severity. The SARS-CoV-2, currently the most pathogenic form compared to SARS-CoV, was identified in 2002, and the Middle East respiratory syndrome coronavirus (MERS-CoV) was reported in 2013 (Chen et al., 2020; Woo et al., 2009).

The sequencing of the SARS-CoV-2 genome (Khailany et al., 2020) has boosted the race to find a protein target for the treatment, whose most promising enzymes are the Spike glycoprotein, which is already used in research for therapeutics and diagnosis, NSP12, also known as RNA-directed RNA polymerase (EC:2.7.7.48), and the main protease NSP5 (M^{pro}), also known as 3 cystein-like proteinase, $3CL^{pro}$ or simply 3CL (EC:3.4.22.69). The M^{pro} acts in the proteolytic processing of replicase polyproteins (pp1a and pp1ab) where, after processing, the pp1a translation products modulate host cell factors, preparing the cell for the synthesis of viral RNA through the formation of replication complexes, while the C-terminal translation products of pp1ab are responsible for the regulation of RNA replication and transcription processes driven by the viral RdRp (nsp12) (Roe et al., 2021). The choice of these enzymes as drug targets is due to the absence of homologous proteins in humans (Anand et al., 2002; Dai et al., 2020).

Among the well-characterized pharmacological targets of coronaviruses, the main protease M^{pro}, of molecular mass of 33.8 kDa, is considered the most promising due to its fundamental role described in the processing of polyproteins that

CONTACT Flavio Augusto Vicente Seixas favseixas@uem.br

Supplemental data for this article can be accessed online at https://doi.org/10.1080/07391102.2023.2166589.

are translated from viral RNA to produce functional viral proteins. This enzyme is mainly involved in the regulation of virion replication and transcription, thus being targeted for research aiming at the design and development of effective therapeutic molecules against Covid-19 (Shamsi et al., 2020).

Due to the urgency in developing effective drugs against covid-19, different strategies were adopted to accelerate the process, such as drug repositioning. This strategy aims to evaluate the effectiveness of drugs already available on the market, which have already undergone clinical tests and have known dosages and side effects (Serafin et al., 2020). In this context, natural products of vegetal origin are an interesting alternative compared to synthetic drugs, as they have been consumed for centuries through traditional medicine and many have also undergone assays that evaluated their toxicity and effectiveness (Gaston et al., 2020; Rao et al., 2019).

Several research groups at the Universidade Estadual de Maringá (UEM), Brazil, and the Instituto Politécnico de Bragança (IPB), Portugal, are dedicated to extracting, chemically characterizing, and testing the functional and antimicrobial properties of plant extracts. The combination of this information allowed the assembling of a library of natural compounds, which is formed by samples of lyophilized and characterized extracts from several plants, among them the purple tea (*Camellia sinensis*) (da Silva et al., 2021); pútegas (*Cytinus hypocistis*) (Silva et al., 2020, 2021), and horse whip (*Luehea divaricata*) (Tanaka et al., 2005).

Among the extracts cited above, the plant *Cytinus hypocistis*, characteristic of the Mediterranea region, was of special interest for the present work. This species has no roots, stems or leaves, with the flowers being the only visible during the reproductive period when they emerge from the host tissues of wild plants belonging to the Cistaceae family (de Vega et al., 2009). The extracts from this plant have gained prominence for their antimicrobial properties, being explored in the treatment of dysentery and for their astringent qualities (Zucca et al., 2015). The biological properties attributed to C. *hypocistis* (antioxidant, antityrosinase, anti-inflammatory, and antibacterial) are associated with its high levels of hydrolyzable tannins, which are a class of phenolic compounds commonly found in plants and studied for their therapeutic activity and enzymatic inhibitory properties (Silva et al., 2021).

The antimicrobial properties of tannins are well known and reported, including their role as a possible antivirals in studies using HIV (Nonaka et al., 1990), HSV (Fukuchi et al., 1989), and hepatitis (Ajala et al., 2014); bacterial diseases caused by *Staphylococcus* strains (Hatano et al., 2005), and parasite diseases (Hoste et al., 2006), which raises the possibility of them being exploited against covid-19.

Considering the antimicrobial properties of tannins and the availability of a library of characterized plant compounds from different research groups (UEM and IPB), the objective of this work was to evaluate the antiviral activity of extracts obtained from *Cytinus hypocistis*, (L.) L. (pútegas), *Camellia sinensis* (L.) Kuntze (purple tea), *Luehea divaricate* Mart. (horse whip) and the compound 1,2,3,4,6-Penta-O-Galloyl-β-d-Glucose (PGG), as SARS-CoV-2 main protease (M^{pro}) inhibitors.

2. Material and methods

2.1. Biological material

The expression vector pET22b(+) containing the gene M^{pro} [Pet22b(+)M^{pro}(His)6x] was purchased from the FastBio company. This vector contains an ampicillin antibiotic resistance gene and encodes a tail with 6 histidine residues (His-tag) at the M^{pro} C-terminal. The bacteria *Escherichia coli*, strain BL21(DE3), which has the T7 RNA polymerase gene under the control of the IPTG (Isopropyl β-D-1-thiogalactopyranoside) inducible lacUV5 promoter was used for the overexpression of the protein of interest. The transformation with the vector occurred by heat shock. The *E. coli* BL21(DE3) cultures transformed with pET22b(+) were grown aerobically in an 1 L Erlenmeyer flask containing 200 mL of Luria Bertani (LB) medium with 50 $\mu g.mL^{-1}$ ampicillin, which was incubated at 37 °C in an orbital shaker at 75 rpm until reaching 0.6 of OD_{600}. Afterward, IPTG was added at a final concentration of 0.5 mM, thus induction at 20 °C for 14 h at 175 rpm. After induction, the culture was centrifuged at 10,000 *g* for 10 min at 4 °C, and the pellet was washed with 10 mM Tris-HCl, pH 8.0, and stored at −20 °C.

In the purification process, the culture pellet was resuspended in binding buffer (50 mM NaH_2PO_4, 300 mM NaCl and 10 mM imidazole, pH 8,0) with 10% glycerol, 0,2% Triton X-100, and 1× protease inhibitor, and sonicated to disrupt the cells in an ice bath for 4 minutes with pulses of 20 sec *On* and 20 sec *Off* with 60% amplitude in a Fisher Scientific sonicator. The disrupted cells were centrifuged at 10,000 *g* for 10 minutes at 4 °C and the supernatant was filtered through a Millex® syringe filter of 0,22 μm (MerckMillipore), for the separation of the soluble protein fraction. Purification of M^{pro} occurred from the soluble fraction through affinity chromatography in an ÄKTA Pure system (GE) using a 1 mL HisTrap column. The sample was injected into the equipment using a 10 mL superloop. The M^{pro} was eluted with elution buffer (50 mM NaH_2PO_4, 300 mM NaCl and 300 mM imidazole, pH 8.0) and purification was confirmed by 12% SDS-PAGE.

The plant extracts from *Cytinus hypocistis* obtained by heat (CHAE), and by ultrasound (CUAE), as well as from *Camellia sinensis* and *Luehea divaricate* were obtained as previously described (da Silva et al., 2021; Silva et al., 2020, 2021; Tanaka et al., 2005). The compound pentagalloyl glucose (PGG) was synthetized by methanolysis of tannic acid as described in the literature (Kato-Schwartz et al., 2018).

2.2. Specific proteolytic activity assay using the fluorogenic substrate

The fluorogenic substrate LGSAVLQ-Rh110-dP (Boston Biochem, USA) was used for the M^{pro} proteolytic assay. This substrate contains the cleavage sequence NSP4/NSP5, GVLQ↓SG19, and acts as a specific peptide substrate for this protease. Fluorescence was measured continuously on a FlexStation 3 plate reader (Molecular Devices, USA) for 5 min. The catalytic activity (reaction rate) in each condition was determined by linear regression in the first 30 seconds reaction.

2.3. The SARS-CoV-2 M^{pro} inhibition assays

The extracts evaluated as inhibitor candidates from the plants *Cytinus hypocistis*, named CHAE (heat extraction) and CUAE (ultrasound extraction), were kindly provided by Dr. Lillian Barros (ICB Bragança, Portugal), while the extracts of horse whip and purple tea, in addition to the PGG compound, were kindly provided by Dr. Rosane Maria Peralta from the Department of Biochemistry at the State University of Maringá (UEM). The assays in the presence of potential inhibitors were the single point, in which a 10 μM of fluorogenic substrate and 1 μM M^{pro} were used in a reaction buffer containing 5 μL inhibitor at a final concentration of 43.8 $\mu g \cdot mL^{-1}$ in a final volume of 300 μL.

The inhibitor candidates were diluted in dimethylsulfoxide (DMSO), which was also tested to evaluate its influence at the rate of the enzymatic reaction. Two control solutions were used, control 1 (Ctrl 1) containing buffer solution in place of the inhibitor and control 2 (Ctrl 2) with 5 μL of pure DMSO in place of the inhibitor. The inhibition rate was calculated in comparison with the Ctrl 2 since DMSO showed inhibitory activity of the enzyme.

The reagents were mixed and pre-incubated for 10 min to reach assay temperature at 37 °C. The reaction started with the addition of M^{pro} enzyme. All runs were subtracted from their respective baselines (all components of each test, except M^{pro}). The reaction take place for 5 min and the fluorescence was read every 10 seconds. The reaction rate in the presence of inhibitors was calculated as described above and the assays were performed in duplicate.

2.4. Assays in cultures of vero cells

The extracts that showed inhibitory activity against M^{pro} were sent for testing for antiviral activity in Vero cells at the laboratory of biosecurity level 3 (NB3), at the University of São Paulo (USP). The compounds were dissolved in DMSO to a concentration of 20 $mg \cdot mL^{-1}$ and were tested in dose-response assays. Before performing cell treatment, compounds were diluted 33.33× in phosphate buffer saline (PBS), and 10 μL of these solutions were transferred to assay plates, thus having a dilution factor of 200×, and chloroquine was used as control. The 384-well plates in DMEM High were used to seed Vero cells, which were incubated for 24 h. After the incubation process (37 °C, 5% CO_2), the compounds were incorporated into the plate to reach a final concentration of 100 $\mu g \cdot mL^{-1}$ (highest concentration tested in the dose-response curve), followed by viral inoculation, where viral particles were added at a multiplicity of the infection (MOI) of 0.1 Plaque Forming Units (PFU) per cells seeded 24 h earlier, corresponding to 200 PFU/well. The final concentration of DMSO in the assay plates was 0.5% (v/v). The plates were incubated for 33 h (37 °C, 5% CO_2) and subsequently fixed with 4% paraformaldehyde (PFA) and subjected to indirect immunofluorescence as indicated in the protocol below. After washing twice with PBS pH 7.4, the plates were blocked with 5% bovine serum albumin (BSA) (Sigma-Aldrich, USA) in PBS (BSA-PBS) for 30 min at room temperature and washed twice with PBS.

Serum from a Brazilian convalescent covid-19 patient diluted 1:1000 in PBS (v/v) or a rabbit polyclonal anti-SARS-CoV-2 nucleocapsid protein antibody (GeneTex, USA) at 2 $\mu g \cdot mL^{-1}$ in PBS were used as a primary antibody to detect SARS-CoV-2 infection in Vero cells. Primary antibodies were incubated for 30 min and the plates were washed twice with PBS.

As secondary antibodies, were used FITC-labeled goat anti-human IgG (Chemicon) or Alexa 488-labeled goat anti-rabbit IgG (Thermo Scientific, USA) diluted at 4 $\mu g \cdot mL^{-1}$ in 5% bovine serum albumin (BSA) in PBS (v/v) and incubated for 30 min. with 5 $\mu g \cdot mL^{-1}$ 4′,6-diamidino-2-phenylindole dihydrochloride (DAPI, Sigma-Aldrich, USA) in PBS to stain the nuclei. Washing was performed twice with PBS and photographed on the Operetta High Content Imaging System (Perkin Elmer, USA) using a 20× magnification objective. Four images were obtained per well. The acquired images were analyzed using the Harmony software (Perkin Elmer, USA), version 3.5.2. Image analysis consisted of identifying and counting Vero cells based on nuclear segmentation and viral infection based on cytoplasmic staining detected by immunofluorescence assay. The parameters measured in each of the wells were: the total number of cells and the total number of infected cells. The reduction in the number of infected cells indicates the percentage of antiviral activity in the samples. From the infected and uninfected controls, the activity of each of the compounds was normalized, as well as the cell survival rate and data analysis was performed with the GraphPad Prism 5 program, as previous described (Freire et al., 2021).

2.5. Docking and molecular dynamics simulations

The crystallographic structure of the SARS-CoV-2 M^{pro} in complex with the non-covalent broad spectrum inhibitor *N-(4-tert-butylphenyl)-N-[(1R)-2-(cyclohexylamino)-2-oxo-1-(pyridin-3-yl)ethyl]-1H-imidazole-4-carboxamide*, named X77 (PDB id: 6W63) was used in the molecular docking simulations. The protocol for each program was defined through the redocking of the X77 ligand (Pubchem CID: 145998279) and considered validated when the superimposing of X77 ligand presented RMSD (Root Mean Square Deviation) lower than 1.5 Å regarding the crystallographic pose, in four repetitions. The standard algorithm for search and ranking was used in Autodock Vina program (Trott & Olson, 2010), with the search box centered on the ligand and defined with dimensions of 15, 20, and 20 Å at *x*, *y*, and *z*, axes respectively. The uff force field (Rappe et al., 2002) was used for energy minimization of the ligands, before conversion to *.pdbqt format. The Molegro program v-6.1 (Bitencourt-Ferreira & de Azevedo, 2019) used the MolDock Simplex Evolution search algorithm (with 30 runs) and the MolDock Score function for scoring, and the results were ranked by the H-bond parameter. The search space of 9 Å radius was centered on the ligand.

The library of compounds from the extract of *C. hypocistis* (Silva et al., 2020, 2021) was built using the entries deposited in PubChem or Zinc15 databases (Table S1, supplementary material). The entries not available in databases were drawn

by the MarvinSketch program (http://www.chemaxon.com) and the addition of hydrogens and the conversion to the 3 D format were performed by the OpenBabel program (O'Boyle et al., 2011). The reference compound X77 was also included in the library to be used as a cut-off. Table S1 (supplementary material) shows the names of the compounds and their respective PubChem CID or Zinc15 ID entries used for the assembling of the library.

Molecular docking simulations were performed in quadruplicate in each program so that the mean relative score for each compound could be calculated from Equation (1) (da Silva et al., 2021) and used in the ranking of compounds. In this equation, the Vina parameter expresses the average score obtained by each molecule using this program, and $Vina_{max}$, is the maximum average score found with this program. The same goes for the term Molegro when using this program.

$$Mean\ relative\ score = \frac{1}{2}\left(\frac{Vina}{Vina_{\max}} + \frac{Molegro}{Molegro_{\max}}\right) \quad (1)$$

To investigate the stability of protein-ligand complexes, molecular dynamics simulations were performed using the program GROMACS 5.1.2 (Van Der Spoel et al., 2005). The M^{pro} monomer complexed with the ligand was used to generate the dimer (biological unit) with the UCSF Chimera program (Pettersen et al., 2004). The dimer was solvated in a periodic box, whose edges were at least 25 Å from the outermost surface of the complex, which had the charges neutralized by the addition of sodium counterions. For the protein, water, and salts, the topology files and parameters associated with the CHARMM36 force field were used (Mackerell et al., 2004). The topology file for the new ligands was generated by the SwissParam server (Zoete et al., 2016). The system was submitted to energy minimization by the steepest descent algorithm, which was terminated after 50,000 steps or when the magnitude of the maximum force on an atom was less than 10 $kJ{\cdot}mol^{-1}{\cdot}nm^{-1}$. In the NVT (constant number of atoms, volume, and temperature) and NPT (constant number of atoms, pressure, and temperature) equilibration steps, the leap-frog algorithm was used to integrate the equations of motion, with a step of 2 fs during 100 ps and, in these steps, the ligand and the protein were kept under movement restrictions. In the NVT step, the Maxwell distribution for velocities was used to implement the temperature of 300 K in the system; in the NPT step, the pressure was set to 1 bar. Finally, the long-term equilibrium dynamics (50 million steps equivalent to 100 ns) in the NPT condition (1 bar and 300 K) were performed, with the ligand and the protein atoms free to move. Simulations were performed in a Dell AMD Epyc 7662/nVIDIA Tesla A100 cluster installed on CENAPAD-SP.

The trajectory file generated by the long-time molecular dynamics simulation was used to calculate the RMSD and radius of gyration parameters throughout the simulation. The last 25 ns of the trajectory file were considered for the estimation of the binding free energy by the MM-PBSA method (Molecular Mechanics Poisson-Boltzmann Surface Area) by the g_mmpbsa program (Kumari et al., 2014).

Table 1. Values of the mean relative score obtained from docking simulations and the change in free energy of binding calculated for the compounds X77 (reference) and Tellimagrandin II.

Compound	Mean relative score	MM-PBSA $\Delta G_{binding}$ (kJ mol^{-1})
X77	0.51	−88.97 ± 8.930
Tellimagrandin II	0.94	−14.98 ± 11.656

3. Results

3.1. Expression and purification of SARS-CoV-2 M^{pro}

The protein expression and purification were confirmed using SDS-PAGE, by comparing the bands obtained with the estimated molecular weight for the protein of interest as 34.9 kDa (Figure 1), predicted by the ProtParam platform. A satisfactory yield was observed in the production of M^{pro}, resulting in approximately 2 mL of pure protein at concentrations ranging between 60 to 80 mg/100 mL of culture. The purity was considered sufficient after affinity chromatography, showing no contaminating bands after sample concentration in a 30 kDa Amicon centrifuge tube, as shown in lane 7 of Figure 1.

3.2. Prospecting SARS-CoV-2 M^{pro} inhibitors

The inhibitory activity of the extracts from *C. hypocistis* CHAE (heat extraction) and CUAE (ultrasound extraction), horse whip, purple tea, and the compound PGG over SARS-CoV-2 M^{pro} was evaluated in a single-point assay (Figure 2), being all samples at the same concentration of 43.8 $\mu g{\cdot}mL^{-1}$. The composition of these extracts differs in the amount and kinds of tannins, being this the reason they were selected for the enzyme inhibition tests among other extracts from the library of natural products of UEM. The sample referring to Control 1 of the reaction does not contain any of the tested compounds nor DMSO, being the condition with less possible interference in the study. In Control 2, DMSO was added in the same concentration used in the assays with the inhibitors, to assess whether there would be any change in M^{pro} activity.

Figure 2A shows the negative influence through the reduction of fluorescence emission caused by the addition of DMSO (diluent of the compounds). Thus, the protease activity in the

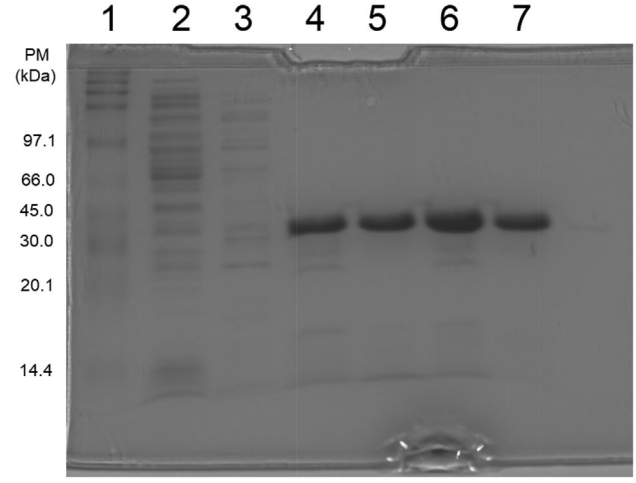

Figure 1. SDS-PAGE 12% after purification of M^{pro}. (1) Molecular weight marker; (2) Flow Through; (3) to (6) samples eluted on HisTrap column 0 to 30% elution buffer; (7) sample concentrated in 30 kDa Amicon centrifuge tubes (final purity).

assays with the inhibitors was represented regarding the activity found in Control 2; therefore, the rates found in the first 30 *sec* of reaction for all compounds were normalized regarding Control 2 (Figure 2B).

Control 1 showed 60% more activity compared to Control 2, showing that DMSO was able to reduce the proteolytic activity of M^{pro} even at low concentrations. The possible reason is the fact that enzymatic activity is directly related to the proper folding of the protein. Therefore, DMSO being a co-solvent widely used for the solubilization of hydrophobic drugs, due to its ability to be miscible in water and most organic liquids, may favor the exposure of hydrophobic residues from inside the protein, affecting the interactions that stabilize it (Modrzyński et al., 2019).

Several studies point out that DMSO, even at low concentrations, can inhibit the activity of several enzymes, including proteases (Kumar & Darreh-Shori, 2017; Modrzyński et al., 2019; Wang et al., 2016). After carrying out the controls, the possibility of DMSO decreasing the M^{pro} activity by absorbing part of fluorescent light was ruled out, since DMSO is optically inert.

Regarding the inhibitory effects, the sample that presented the highest inhibitory activity over M^{pro} was the CUAE extract, inhibiting more than 90% activity. Since it presented the best inhibition results, the ultrasonically extracted *Cytinus hypocistis* extract (CUAE) was selected for assays on Vero cells infected with SARS-CoV-2.

3.3. Cytotoxicity and antiviral activity assays in vero cells

The concentration of CUAE that causes a 50% reduction in cell viability (CC_{50}) when compared to the cytotoxicity control, as well as the concentration of the compound responsible for the 50% inhibition of viral replication (EC_{50}) when compared to the viral control, were determined through the analysis of the nonlinear regression of the dose-response curve, through the GraphPad Prism 5 program, as shown in Figure 3.

The CUAE extract caused 99.6% inhibition of viral activity compared to the control. Regarding cytotoxicity, the evaluated compound presented $CC_{50} > 100.00\ \mu g{\cdot}mL^{-1}$, being above the detection limit of the method. This value is not comparable with that of Chloroquine, since both are in different concentration units; however, this value is important to evaluate the selectivity index (SI). This index is extremely important to ensure that the inhibition caused by a substance is due to the activity of the virus and not due to toxicity on the host cells (Marcovicz et al., 2018). The ideal for a compound to be considered a hit for a new drug is that its selectivity index is greater than or equal to 10 (Indrayanto et al., 2021). Thus, with a selectivity index greater than 40, the CUAE extract suggests a potential candidate for developing new drugs for the treatment of SARS-CoV-2 infections since it presented maximum activity and SI practically equal to those of chloroquine. Since it is a heterogeneous plant extract, the concentration of CUAE was expressed in $\mu g{\cdot}mL^{-1}$, while the concentration of the control chloroquine was expressed in μM. This makes the SI parameters and maximum activity the most important in this assay.

3.4. Docking and molecular dynamics of C. hypocistis extract compounds

The library of the compounds from the extract of *C. hypocistis* was subjected to molecular docking simulations through the programs Vina and Molegro, having the M^{pro} structure of SARS-CoV-2 as a target. As a result, the compounds CID65238 and CID374874, isomers of pentagalloylglucose (PGG), had the highest mean relative score (Figure 4). However, it was not possible to identify a pattern in the docking poses of these compounds at the active site of the target (Figure S1, Supplementary material). This indicates the absence of a site-specific binding pattern on M^{pro}, which would be the expected behavior for a drug-like ligand. However, the compound Tellimagrandin II (CID151590) presented the third highest mean relative score (Figure 4), and the docking simulations present the same poses in every attempt using both Molegro and Vina programs (Figure 5A). This result makes it possible to predict the conformation of the compound in the active site and to analyze the interactions it makes with M^{pro} (Figure 5B). This is a pattern behavior that is expected for a drug-like ligand. The visual inspection shows that Telligramandin II establishes several hydrogen interactions with

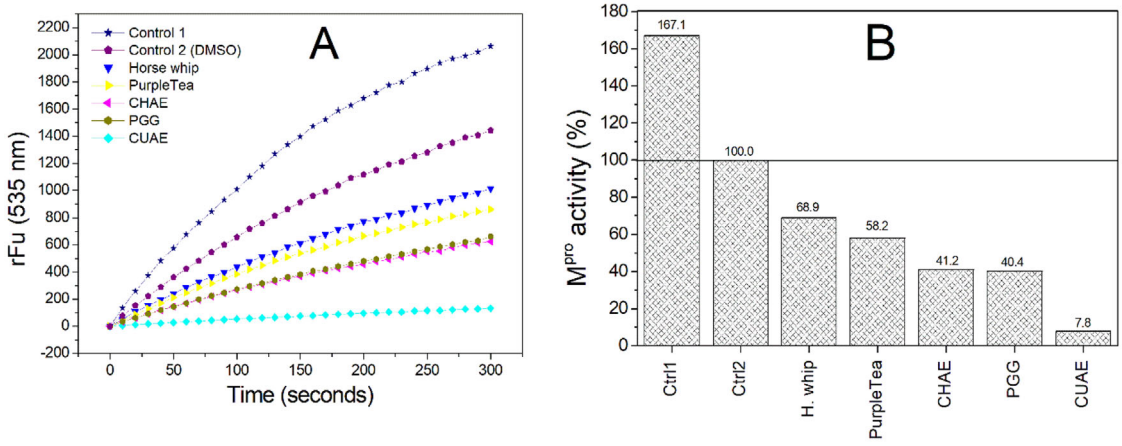

Figure 2. (A) Evaluation of SARS-CoV-2 M^{pro} inhibition by the five extracts evaluated: CUAE and CHAE from *Cytinus hypocistis*, Purple tea (*Camellia sinensis*), Horse whip (*Luehea divaricata*), and the compound PGG (pentagalloylglucose). The assay was monitored for 300 seconds at 535 nm. (B) The activity of the five tested compounds normalized regarding Control 2. Reaction buffer was 50 mM Tris-HCl, pH 7.5, 1 mM EDTA. The enzyme concentration was 1 μM, fluorogenic substrate at a concentration of 10 μM, and the extracts at 43.8 $\mu g.mL^{-1}$.

Compound ID	EC_{50}	CC_{50}	SI	Max. Activity (%)	DRCs
Chloroquine µM	0.69	30.42	44.3	99.0	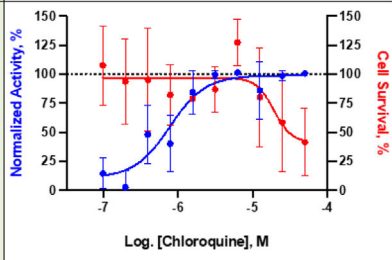
CUAE µg/mL	2.34	> 100.00	42.7	99.6	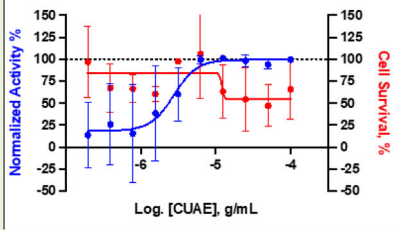

Figure 3. Results of antiviral activity and cytotoxicity assays. The selectivity index (SI) is determined by the CC_{50}/EC_{50} ratio. The compound chloroquine was used as a reference.

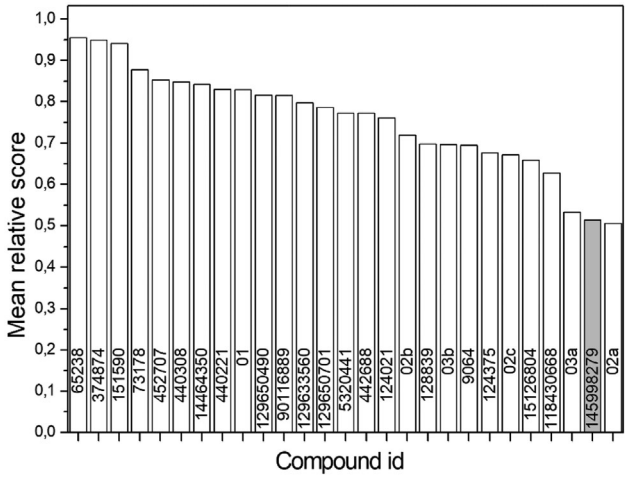

Figure 4. Mean relative score obtained from docking of the compounds from *C. hypocistis* extract with SARS-CoV-2 M^{pro}. The grey bar is the reference ligand X77 (CID 145998279). A list of compound names is given in Table S1, supplementary material.

M^{pro} residues, including the Cys145, which is part of the catalytic dyad of the enzyme (Kneller et al., 2020). The high mean relative score and the occurrence of a binding conformation pattern in the active site suggest the compound Tellimagrandin II as the most likely inhibitor of M^{pro}.

The complexes constituted by the SARS-CoV-2 M^{pro} dimer associated with the reference ligand X77 (M^{pro}-X77) and the Tellimagrandin II compound (M^{pro}-TellimagrandinII) were submitted to molecular dynamics simulation using the GROMACS program. Since, there is no way to know which pose of the PGG we would have to use in the MD, and the same with the other components of the extract, we proceed with MD only with Tellimagrandin II. The temporal evolution of the radius of gyration and RMSD parameters for the main chain atoms of the protein indicate the stability of the M^{pro} dimer during the simulation in the two evaluated complexes (Figure 6A and B). The ligands X77 and Tellimagrandin II stay in the active site of M^{pro}, as indicated by the stability of the RMSD parameter for the compounds throughout the simulation (Figure 6B), which suggests the stability of the protein-ligand complex in the two systems evaluated. From the trajectory file obtained in the simulation of long-time equilibrium dynamics (NPT), the binding free energy associated with the M^{pro}-X77 and M^{pro}-Tellimagrandin II complexes was calculated by the MM-PBSA method (Table 1). The values of $\Delta G_{binding}$ calculated for the M^{pro} ligands indicate that Tellimagrandin II would have a lower affinity than the reference ligand X77 ($IC_{50} = 2.3\,\mu M$ from PDB entry), which is in agreement with the data observed in our *in vitro* assays.

The data in Table 1 show that the mean relative score for the Tellimagrandin II ligand is higher than that for the X77. Although this result indicates a higher binding probability for Tellimagrandin II, this result is less accurate than the $\Delta G_{binding}$ calculated by the MM-PBSA method. It also implicates that the scores provided by docking programs should not be misinterpreted as $\Delta G_{binding}$.

4. Discussion

The *C. hypocistis* is a wild parasitic plant, whose extract has already been characterized and is known for its high levels of tannins, which can give the plant extracts bioactive and inhibitory properties of some enzymes (Silva et al., 2021). Tannins are polyphenols of great economic and ecological interest. These compounds are soluble in water and have a molecular weight ranging from 500 to 3,000 Daltons, forming water-insoluble complexes with proteins, gelatins, and alkaloids (Chung et al., 1998). The binding between tannins and proteins possibly, happens through the hydrogen bonds between the hydroxyl of the phenolic groups of the tannins and certain sites of the proteins, giving greater stability to these substances (Hagerman & Klucher, 1986).

Many studies point to the biological activity of tannins against certain microorganisms, which may act as anti-inflammatory (Koleckar et al., 2008), healing (Pellenz et al., 2019), and even as HIV reverse transcriptase inhibitors (Nonaka et al., 1990).

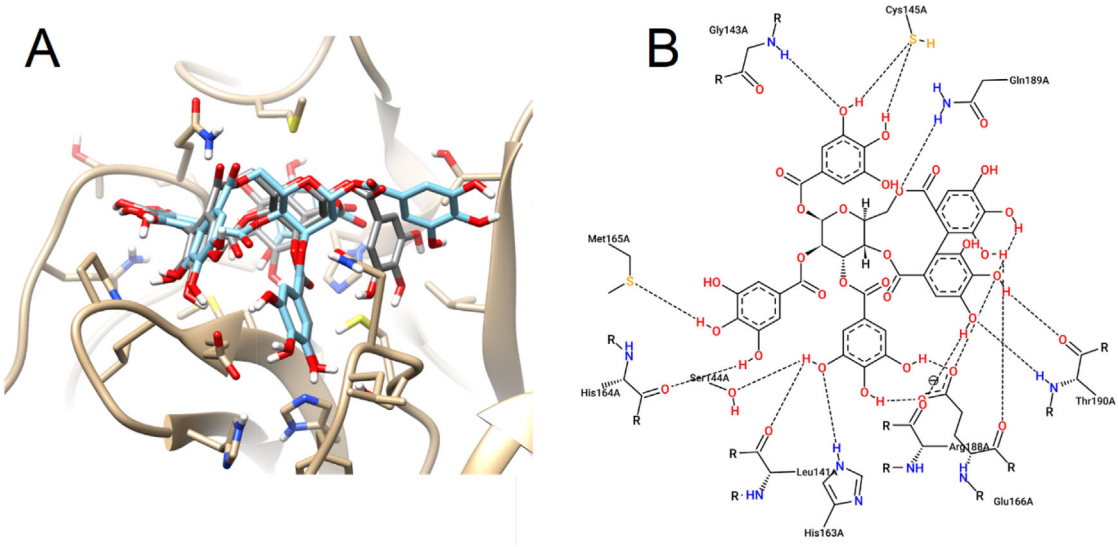

Figure 5. **(A)** The best pose of the Tellimagrandin II compound docked at the SARS-CoV-2 M^{pro} active site as predicted by Molegro (grey) and Vina (blue) programs. **(B)** A 2 D diagram of interactions between the compound Tellimagrandin II and M^{pro} is described by the PoseView program (Stierand et al., 2006).

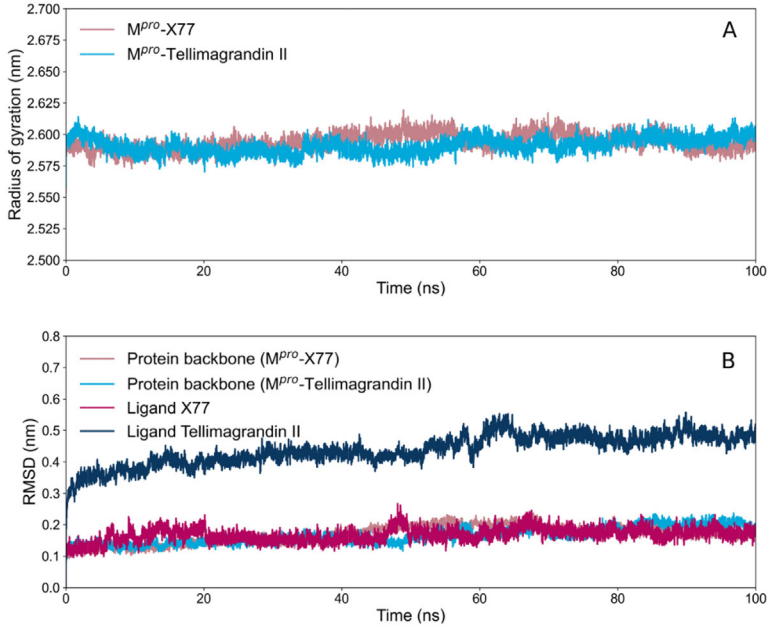

Figure 6. Time evolution of the parameter radius of gyration **(A)** and RMSD **(B)** for the M^{pro} dimer complex with ligand X77 or Tellimagrandin II. Values were calculated for the protein main chain atoms (backbone) and for the X77 and Tellimagrandin II ligands in the respective dimers.

There are probably two different ways that tannins can exert their biological effects. The first in its non-absorbable form as a complex structure, generating antioxidant, antimicrobial, antiviral, antimutagenic, and antinutritional effects locally, still in the gastrointestinal tract, or in the absorbable form arising from the fermentation of tannins, which can produce generalized effects in various organs (Al-Ishaq et al., 2020; Chung et al., 1998; Kawabata et al., 2019).

The applications of tannins as drugs are mainly related to their astringent properties. Through the precipitation of proteins, tannins provide an antimicrobial and antifungal effect. Several bacteria are sensitive to tannins, including *Staphylococcus aureus*, *Streptococcus pneumonia*, *Bacillus anthracis,* and *Shigella dysenteriae* (Scalbert, 1991) and, at minimal concentrations (0.5 g/L), the fungus *Fomes annosus* had its growth inhibited (Haars et al., 1981).

Due to the different effects of tannins on proteins, as well as the fact that our cell assays were performed with the addition of tannins before the addition of the virus, it is not possible to assert which mechanism caused the observed antiviral effect. Some of the tannins may have bound to the ACE2 protein of the Vero cell, or the spike protein of SARS-CoV-2, to prevent the virus from fusing with the host cell. It is also possible and much more likely, that Tellimagrandin II was bound to M^{pro}, as demonstrated by the inhibitory effect on this enzyme by our *in vitro* assays. It is noteworthy that the tannin composition of the heat-extracted extract (CHAE) is the same as that of the ultrasonic-extracted extract (CUAE), with small variations in the concentrations of each component; however, it is not a significant difference (± 5%) (Silva et al., 2021). This suggests that heat extraction may have affected the extract components in some way compared to ultrasound extraction, probably by

oxidation/degradation of the active component, which may be the cause of the difference in the M^{pro} inhibitory activity observed in Figure 2.

The *in silico* study indicated PGG as the most likely inhibitor of M^{pro} among the compounds in the library; however, in its pure form, PGG was able to inhibit around 60% of the enzyme activity (Figure 2). In spite this number represents a significant inhibition, it does not justify how CUAE extract, which contains a smaller amount of PGG than the one used in pure form in enzyme assays, managed to inhibit 92% of the M^{pro} activity. In addition, the suggestion by docking that PGG does not bind to M^{pro} through a specific pose (Figure S1, supplementary material) reinforces the hypothesis that PGG acts promiscuously to different enzymes (Szabó et al., 2021). On the other hand, Tellimagrandin II, a compound also present in the extract of *C. hypocistis* (Silva et al., 2020), gains strength as the most likely inhibitor of M^{pro}. It is an interesting fact that this compound was present and also identified as the likely inhibitor of M^{pro} in studies using the Sibipiruna extract (*Cenostigma pluviosum* var. *peltophoroides*) in similar work (Pattaro-Júnior et al., 2022). It is also an interesting fact that Tellimagrandin II is not present in the extracts of *C. sinensis* nor *Luehea divaricate*, which did not show significant inhibition of M^{pro} in the enzymatic assays in this work. In short only extracts that have Tellimagrandin II among their components appear to inhibit M^{pro}. Added to this, the fact that the same docking pose for Tellimagrandin II in the active site of the M^{pro} has been identified by different docking programs from different simulation attempts (Figure 5) suggests a behavior expected for a drug-like ligand. The molecular dynamics simulations of M^{pro} bounded to Tellimagrandin II indicate that the complex is stable and the ligand remains in a fixed position in the active site throughout the simulation (Figure 6), which reinforces the hypothesis that Tellimagrandin II interact as drug-like. Even so, we cannot rule out the possibility that PGG and Tellimagrandin II act in synergism to inhibit M^{pro}.

The literature reports that the compound Tellimagrandin II isolated from the plant *Geum japonicum* showed mixed non-competitive inhibition of thrombin, which confers anticoagulant activity to it (Dong et al., 1998). In severe cases of covid-19, the cytokine storm induced by the viral infection ends up activating the coagulation cascade leading to thrombotic events, so the use of anticoagulants has been considered in the treatment of the disease (Sholzberg et al., 2021). In this context, the Tellimagrandin II compound could stand out as a promising candidate for the treatment of covid-19 due to its antiviral and anticoagulant activities.

The cytokine storm also causes generalized inflammatory processes that improve after treatment with steroidal anti-inflammatory drugs (Sanders et al., 2020). The high levels of hydrolyzable tannins present in *C. hypocistis* (Silva et al., 2021) may contribute to an improvement in the inflammatory condition generated by covid-19, given the antioxidant and anti-inflammatory activity of tannins. This could reduce the morbidity and mortality in cases of this disease due to its role in maintaining redox homeostasis (Goli, 2020). However, this hypothesis needs to be tested through assays in animal infection models, which are already underway by our research group.

In summary, the results presented in this work are considered promising, as they showed a compound capable of inhibiting 99.6% of viral infections in a non-tumor cell line. It also evidenced the need for further studies to clarify the mechanism of action of the plant compounds against the viral protease. Our results also indicate the need to identify the fractions of *C. hypocistis* to isolate the compound responsible for the viral infection inhibition, thus, decreasing possible toxic effects. This may imply Tellimagrandin II or an isolated fraction of the *C. hypocistis* extract to be evaluated as a treatment option against covid-19 in the future.

5. Conclusion

The results presented in this work indicate that the extract of *C. hypocistis*, obtained using the ultrasound technique (CUAE) is a good M^{pro} inhibitor and showed potent antiviral activity in Vero cells infected with SARS-CoV-2. The tannins present in the extract of *C. hypocistis* have an evident antiviral action, suggesting that the extract is a possible candidate for the development of herbal drugs against the infection caused by SARS-CoV-2. This is an important discovery given the current scarcity of specific medicines in the market to treat severe cases of covid-19.

Disclosure statement

No potential conflict of interest was reported by the authors.

Funding

This work was funded by Coordination for the Improvement of Higher Education Personnel - Brazil (CAPES) - Code 001 and project number 88887.505029/2020-00, and by Araucária Foundation (agreement 87/2021). The authors thank FINEP and COMCAP/UEM for the facilities, and CENAPAD/SP for the computational resources (projects 520 and 870). The authors are grateful to the Foundation for Science and Technology (FCT, Portugal) for financial support through national funds FCT/MCTES (PIDDAC) to CIMO (UIDB/00690/2020 and UIDP/00690/2020) and SusTEC (LA/P/0007/2020). A. R. Silva is grateful to FCT and FSE for her Doctoral Grant (SFRH/BD/145834/2019) and L. Barros for her contract through the institutional scientific employment program-contract.

ORCID

Gisele Strieder Philippsen http://orcid.org/0000-0002-4725-2323
Lillian Barros http://orcid.org/0000-0002-9050-5189
Maria Aparecida Fernandez http://orcid.org/0000-0002-7696-5680
Flavio Augusto Vicente Seixas http://orcid.org/0000-0002-0117-6919

References

Ajala, O. S., Jukov, A., & Ma, C.-M. (2014). Hepatitis C virus inhibitory hydrolysable tannins from the fruits of Terminalia chebula. *Fitoterapia*, *99*, 117–123. https://doi.org/10.1016/j.fitote.2014.09.014

Al-Ishaq, R. K., Overy, A. J., & Büsselberg, D. (2020). Phytochemicals and gastrointestinal cancer: Cellular mechanisms and effects to change cancer progression. *Biomolecules*, *10*(1), 105. https://doi.org/10.3390/biom10010105

Anand, K., Palm, G. J., Mesters, J. R., Siddell, S. G., Ziebuhr, J., & Hilgenfeld, R. (2002). Structure of coronavirus main proteinase reveals combination of a chymotrypsin fold with an extra alpha-helical

domain. *The EMBO Journal*, *21*(13), 3213–3224. https://doi.org/10.1093/emboj/cdf327

Bitencourt-Ferreira, G., & de Azevedo, W. F. (2019). Molegro virtual docker for docking. *Methods in Molecular Biology (Clifton, N.J.)*, *2053*, 149–167. https://doi.org/10.1007/978-1-4939-9752-7_10

Chen, Y., Liu, Q., & Guo, D. (2020). Emerging coronaviruses: Genome structure, replication, and pathogenesis. *Journal of Medical Virology*, *92*(4), 418–423. https://doi.org/10.1002/jmv.25681

Chung, K.-T., Wong, T. Y., Wei, C.-I., Huang, Y.-W., & Lin, Y. (1998). Tannins and human health: A review. *Critical Reviews in Food Science and Nutrition*, *38*(6), 421–464. https://doi.org/10.1080/10408699891274273

da Silva, T. B. V., Castilho, P. A., Sá-Nakanishi, A. B. d., Seixas, F. A. V., Dias, M. I., Barros, L., Ferreira, I. C. F. R., Bracht, A., & Peralta, R. M. (2021). The inhibitory action of purple tea on in vivo starch digestion compared to other Camellia sinensis teas. *Food Research International (Ottawa, Ont.)*, *150*, 110781. https://doi.org/10.1016/j.foodres.2021.110781

Dai, W., Zhang, B., Jiang, X.-M., Su, H., Li, J., Zhao, Y., Xie, X., Jin, Z., Peng, J., Liu, F., Li, C., Li, Y., Bai, F., Wang, H., Cheng, X., Cen, X., Hu, S., Yang, X., Wang, J., … Liu, H. (2020). Structure-based design of antiviral drug candidates targeting the SARS-CoV-2 main protease. *Science (New York, N.Y.)*, *368*(6497), 1331–1335. https://doi.org/10.1126/science.abb4489

de Vega, C., Arista, M., Ortiz, P. L., Herrera, C. M., & Talavera, S. (2009). The ant-pollination system of Cytinus hypocistis (Cytinaceae), a Mediterranean root holoparasite. *Annals of Botany*, *103*(7), 1065–1075. https://doi.org/10.1093/aob/mcp049

Dong, H., Chen, S.-X., Kini, R. M., & Xu, H.-X. (1998). Effects of tannins from *Geum japonicum* on the catalytic activity of thrombin and factor Xa of blood coagulation cascade. *Journal of Natural Products*, *61*(11), 1356–1360. https://doi.org/10.1021/np9801458

Freire, M. C. L. C., Noske, G. D., Bitencourt, N. V., Sanches, P. R. S., Santos-Filho, N. A., Gawriljuk, V. O., de Souza, E. P., Nogueira, V. H., de Godoy, M. O., Nakamura, A. M., & Fernandes, R. S. (2021). Non-toxic dimeric peptides derived from the bothropstoxin-I are potent SARS-CoV-2 and papain-like protease inhibitors. *Molecules*, *26*(16), 4896. https://doi.org/10.3390/molecules26164896

Fukuchi, K., Sakagami, H., Okuda, T., Hatano, T., Tanuma, S., Kitajima, K., Inoue, Y., Inoue, S., Ichikawa, S., & Nonoyama, M. (1989). Inhibition of herpes simplex virus infection by tannins and related compounds. *Antiviral Research*, *11*(5–6), 285–297. https://doi.org/10.1016/0166-3542(89)90038-7

Gaston, T. E., Mendrick, D. L., Paine, M. F., Roe, A. L., & Yeung, C. K. (2020). "Natural" is not synonymous with "Safe": Toxicity of natural products alone and in combination with pharmaceutical agents. *Regulatory Toxicology and Pharmacology*, *113*, 104642. https://doi.org/10.1016/j.yrtph.2020.104642

Goli, M. (2020). Review of novel human β-coronavirus (2019-nCoV or SARS-CoV-2) from the food industry perspective—Appropriate approaches to food production technology. *Food Science & Nutrition*, *8*(10), 5228–5237. https://doi.org/10.1002/fsn3.1892

Haars, A., Chet, I., & Hüttermann, A. (1981). Effect of phenolic compounds and tannin on growth and laccase activity of Fomes annosus. *Forest Pathology*, *11*(1–2), 67–76. https://doi.org/10.1111/j.1439-0329.1981.tb00072.x

Hagerman, A. E., & Klucher, K. M. (1986). Tannin-protein interactions. *Progress in Clinical and Biological Research*, *213*, 67–76. http://www.ncbi.nlm.nih.gov/pubmed/3520596

Hatano, T., Kusuda, M., Inada, K., Ogawa, T., Shiota, S., Tsuchiya, T., & Yoshida, T. (2005). Effects of tannins and related polyphenols on methicillin-resistant Staphylococcus aureus. *Phytochemistry*, *66*(17), 2047–2055. https://doi.org/10.1016/j.phytochem.2005.01.013

Hoste, H., Jackson, F., Athanasiadou, S., Thamsborg, S. M., & Hoskin, S. O. (2006). The effects of tannin-rich plants on parasitic nematodes in ruminants. *Trends in Parasitology*, *22*(6), 253–261. https://doi.org/10.1016/j.pt.2006.04.004

Huang, C., Wang, Y., Li, X., Ren, L., Zhao, J., Hu, Y., Zhang, L., Fan, G., Xu, J., Gu, X., & Cheng, Z. (2020). Clinical features of patients infected with 2019 novel coronavirus in Wuhan, China. *The Lancet*, *395*(10223), 497–506. https://doi.org/10.1016/S0140-6736(20)30183-5

Indrayanto, G., Putra, G. S., & Suhud, F. (2021). Validation of in-vitro bioassay methods: Application in herbal drug research. *Profiles of Drug Substances, Excipients and Related Methodology*, *46*(2021), 273–307. https://doi.org/10.1016/bs.podrm.2020.07.005

Kato-Schwartz, C. G., Bracht, F., de Almeida Gonçalves, G., Soares, A. A., Vieira, T. F., Brugnari, T., Bracht, A., & Peralta, R. M. (2018). Inhibition of α-amylases by pentagalloyl glucose: Kinetics, molecular dynamics and consequences for starch absorption. *Journal of Functional Foods*, *44*, 265–273.

Kawabata, K., Yoshioka, Y., & Terao, J. (2019). Role of intestinal microbiota in the bioavailability and physiological functions of dietary polyphenols. *Molecules*, *24*(2), 370. https://doi.org/10.3390/molecules24020370

Khailany, R. A., Safdar, M., & Ozaslan, M. (2020). Genomic characterization of a novel SARS-CoV-2. *Gene Reports*, *19*, 100682. https://doi.org/10.1016/j.genrep.2020.100682

Kneller, D. W., Phillips, G., O'Neill, H. M., Jedrzejczak, R., Stols, L., Langan, P., Joachimiak, A., Coates, L., & Kovalevsky, A. (2020). Structural plasticity of SARS-CoV-2 3CL Mpro active site cavity revealed by room temperature X-ray crystallography. *Nature Communications*, *11*(1), 3202. https://doi.org/10.1038/s41467-020-16954-7

Koleckar, V., Kubikova, K., Rehakova, Z., Kuca, K., Jun, D., Jahodar, L., & Opletal, L. (2008). Condensed and hydrolysable tannins as antioxidants influencing the health. *Mini Reviews in Medicinal Chemistry*, *8*(5), 436–447. https://doi.org/10.2174/138955708784223486

Kumar, A., & Darreh-Shori, T. (2017). DMSO: A mixed-competitive inhibitor of human acetylcholinesterase. *ACS Chemical Neuroscience*, *8*(12), 2618–2625. https://doi.org/10.1021/acschemneuro.7b00344

Kumari, R., Kumar, R., Lynn, A., & Consort, O. (2014). g_mmpbsa-A GROMACS tool for high-throughput MM-PBSA calculations. *Journal of Chemical Information and Modeling*, *54*(7), 1951–1962. https://doi.org/10.1021/Ci500020m

Mackerell, A. D., Feig, M., & Brooks, C. L. (2004). Extending the treatment of backbone energetics in protein force fields: Limitations of gas-phase quantum mechanics in reproducing protein conformational distributions in molecular dynamics simulations. *Journal of Computational Chemistry*, *25*(11), 1400–1415. https://doi.org/10.1002/jcc.20065

Marcovicz, C., Ferreira, R. C., Santos, A. B. S., Reyna, A. S., de Araújo, C. B., Malvestiti, I., & Falcão, E. H. L. (2018). Nonlinear optical behavior of two tetrathiafulvalene derivatives in the picosecond regime. *Chemical Physics Letters*, *702*, 16–20. https://doi.org/10.1016/J.CPLETT.2018.04.053

Modrzyński, J. J., Christensen, J. H., & Brandt, K. K. (2019). Evaluation of dimethyl sulfoxide (DMSO) as a co-solvent for toxicity testing of hydrophobic organic compounds. *Ecotoxicology (London, England)*, *28*(9), 1136–1141. https://doi.org/10.1007/s10646-019-02107-0

Nonaka, G., Nishioka, I., Nishizawa, M., Yamagishi, T., Kashiwada, Y., Dutschman, G. E., Bodner, A. J., Kilkuskie, R. E., Cheng, Y. C., & Lee, K. H. (1990). Anti-aids agents, 2: Inhibitory effect of tannins on HIV reverse transcriptase and HIV replication in H9 lymphocyte cells. *Journal of Natural Products*, *53*(3), 587–595. https://doi.org/10.1021/np50069a008

O'Boyle, N. M., Banck, M., James, C. A., Morley, C., Vandermeersch, T., & Hutchison, G. R. (2011). Open Babel: An open chemical toolbox. *Journal of Cheminformatics*, *13*(1), 1–14. https://doi.org/10.1186/1758-2946-3-33

Pattaro-Júnior, J. R., Araújo, I. G., Moraes, C. B., Barbosa, C. G., Philippsen, G. S., Freitas-Junior, L. H., Guidi, A. C., de Mello, J. C. P., Peralta, R. M., Fernandez, M. A., & Teixeira, R. R. (2022). Antiviral activity of Cenostigma pluviosum var. peltophoroides extract and fractions against SARS-CoV-2. *Journal of Biomolecular Structure & Dynamics*. https://doi.org/10.1080/07391102.2022.2120078.

Pellenz, N. L., Barbisan, F., Azzolin, V. F., Santos Marques, L. P., Mastella, M. H., Teixeira, C. F., Ribeiro, E. E., & da Cruz, I B. M. (2019). Healing activity of Stryphnodendron adstringens (Mart.), a Brazilian tannin-rich species: A review of the literature and a case series. *Wound Medicine*, *26*(1), 100163. https://doi.org/10.1016/j.wndm.2019.100163

Pettersen, E. F., Goddard, T. D., Huang, C. C., Couch, G. S., Greenblatt, D. M., Meng, E. C., & Ferrin, T. E. (2004). UCSF Chimera?A visualization system for exploratory research and analysis. *Journal of Computational Chemistry*, *25*(13), 1605–1612. https://doi.org/10.1002/jcc.20084

Rao, T., Tan, Z., Peng, J., Guo, Y., Chen, Y., Zhou, H., & Ouyang, D. (2019). The pharmacogenetics of natural products: A pharmacokinetic and pharmacodynamic perspective. *Pharmacological Research*, *146*, 104283. https://doi.org/10.1016/j.phrs.2019.104283

Rappe, A. K., Casewit, C. J., Colwell, K. S., Goddard, W. A., & Skiff, W. M. (2002). UFF, a full periodic table force field for molecular mechanics

and molecular dynamics simulations. *Journal of the American Chemical Society*, *114*(25), 10024–10035. https://doi.org/10.1021/JA00051A040

Roe, M. K., Junod, N. A., Young, A. R., Beachboard, D. C., & Stobart, C. C. (2021). Targeting novel structural and functional features of coronavirus protease nsp5 (3CLpro, Mpro) in the age of COVID-19. *Journal of General Virology*, *102*(3), 001558. https://doi.org/10.1099/jgv.0.001558

Sanders, J. M., Monogue, M. L., Jodlowski, T. Z., & Cutrell, J. B. (2020). Pharmacologic treatments for coronavirus disease 2019 (COVID-19). *JAMA*, *323*(18), 1824-1836. https://doi.org/10.1001/jama.2020.6019

Scalbert, A. (1991). Antimicrobial properties of tannins. *Phytochemistry*, *30*(12), 3875–3883. https://doi.org/10.1016/0031-9422(91)83426-L

Serafin, M. B., Bottega, A., Foletto, V. S., da Rosa, T. F., Hörner, A., & Hörner, R. (2020). Drug repositioning is an alternative for the treatment of coronavirus COVID-19. *International Journal of Antimicrobial Agents*, *55*(6), 105969. https://doi.org/10.1016/j.ijantimicag.2020.105969

Shamsi, A., Mohammad, T., Anwar, S., AlAjmi, M. F., Hussain, A., Rehman, M. T., Islam, A., & Hassan, M. I. (2020). Glecaprevir and Maraviroc are high-affinity inhibitors of SARS-CoV-2 main protease: Possible implication in COVID-19 therapy. *Bioscience Reports*, *40*(6), BSR20201256. https://doi.org/10.1042/BSR20201256

Sholzberg, M., Tang, G. H., Rahhal, H., AlHamzah, M., Kreuziger, L. B., Áinle, F. N., Alomran, F., Alayed, K., Alsheef, M., AlSumait, F., & Pompilio, C. E. (2021). Effectiveness of therapeutic heparin versus prophylactic heparin on death, mechanical ventilation, or intensive care unit admission in moderately ill patients with covid-19 admitted to hospital: RAPID randomised clinical trial. *BMJ*, *375*(n2400). https://doi.org/10.1136/bmj.n2400

Silva, A. R., Pinela, J., Dias, M. I., Calhelha, R. C., Alves, M. J., Mocan, A., García, P. A., Barros, L., & Ferreira, I. C. F. R. (2020). Exploring the phytochemical profile of Cytinus hypocistis (L.) L. as a source of health-promoting biomolecules behind its in vitro bioactive and enzyme inhibitory properties. *Food and Chemical Toxicology*, *136*, 111071. https://doi.org/10.1016/j.fct.2019.111071

Silva, A. R., Pinela, J., García, P. A., Ferreira, I. C. F. R., & Barros, L. (2021). Cytinus hypocistis (L.) L.: Optimised heat/ultrasound-assisted extraction of tannins by response surface methodology. *Separation and Purification Technology*, *276*, 119358. https://doi.org/10.1016/j.seppur.2021.119358

Stierand, K., Maass, P. C., & Rarey, M. (2006). Molecular complexes at a glance: Automated generation of two-dimensional complex diagrams. *Bioinformatics*, *22*(14), 1710–1716. https://doi.org/10.1093/bioinformatics/btl150

Szabó, K., Hámori, C., & Gyémánt, G. (2021). Gallotannins are non-specific inhibitors of α-amylase: Aggregates are the active species taking part in inhibition. *Chemical Biology & Drug Design*, *97*(2), 349–357. https://doi.org/10.1111/cbdd.13787

Tanaka, J. C. A., Silva, C. C. D., Dias Filho, B. P., Nakamura, C. V., Carvalho, J. E. D., & Foglio, M. A. (2005). Constituintes químicos de Luehea divaricata Mart. (Tiliaceae). *Química Nova*, *28*(5), 834–837. https://doi.org/10.1590/S0100-40422005000500020

Trott, O., & Olson, A. J. (2010). AutoDock Vina: Improving the speed and accuracy of docking with a new scoring function, efficient optimization, and multithreading. *Journal of Computational Chemistry*, *31*(2), 455–461. https://doi.org/10.1002/jcc.21334

Van Der Spoel, D., Lindahl, E., Hess, B., Groenhof, G., Mark, A. E., & Berendsen, H. J. C. (2005). GROMACS: Fast, flexible, and free. *Journal of Computational Chemistry*, *26*(16), 1701–1718. https://doi.org/10.1002/jcc.20291

Wang, S., Meng, X., Zhou, H., Liu, Y., Secundo, F., & Liu, Y. (2016). Enzyme stability and activity in non-aqueous reaction systems. *A Mini Review. Catalysts*, *6*(2), 32. https://doi.org/10.3390/catal6020032

Woo, P. C. Y., Lau, S. K. P., Huang, Y., & Yuen, K.-Y. (2009). Coronavirus diversity, phylogeny and interspecies jumping. *Experimental Biology and Medicine (Maywood, N.J.)*, *234*(10), 1117–1127. https://doi.org/10.3181/0903-MR-94

Zoete, V., Daina, A., Bovigny, C., & Michielin, O. (2016). SwissSimilarity: A web tool for low to ultra high throughput ligand-based virtual screening. *Journal of Chemical Information and Modeling*, *56*(8), 1399–1404. https://doi.org/10.1021/acs.jcim.6b00174

Zucca, P., Pintus, M., Manzo, G., Nieddu, M., Steri, D., & Rinaldi, A. C. (2015). Antimicrobial, antioxidant and anti-tyrosinase properties of extracts of the Mediterranean parasitic plant Cytinus hypocistis. *BMC Research Notes*, *8*(1), 562. https://doi.org/10.1186/s13104-015-1546-5